Sensors and Actuators A 187 (2012) 73–78

Contents lists available at SciVerse ScienceDirect

Sensors and Actuators A: Physical

journal homepage: www.elsevier.com/locate/sna

Synthesis of multiwalled carbon nanotube-based infrared radiation detector

Rahat Afrin[a], Jibran Khaliq[b], Mohammad Islam[b,c], Iftikhar Hussain Gul[b], Arshad Saleem Bhatti[d], Umair Manzoor[d,e,*]

[a] Thin Film Technology Laboratory, Department of Physics, COMSATS Institute of Information Technology, Islamabad, Pakistan
[b] School of Chemical and Materials Engineering, National University of Sciences and Technology (NUST), 44000, Islamabad, Pakistan
[c] Center of Excellence for Research in Engineering Materials (CEREM), College of Engineering, King Saud University, P.O. Box 800, Riyadh 11421, Saudi Arabia
[d] Centre for Micro & Nano Devices, Department of Physics, COMSATS Institute of Information Technology, Islamabad, Pakistan
[e] Alamoudi Water Chair, King Saud University, P.O. Box 2460, Riyadh, Saudi Arabia

ARTICLE INFO

Article history:
Received 26 March 2012
Received in revised form 7 August 2012
Accepted 18 August 2012
Available online xxx

Keywords:
MWCNTs
Twisted CNTs
IR sensor

ABSTRACT

Different morphologies (worm-like, straight and twisted) of multiwalled carbon nanotubes (MWCNT) are synthesized by carefully controlling the C_2H_2 flow rate. Unique mixed ferrite nanoparticles were synthesized and characterized as the appropriate catalyst for the growth of MWCNT. Scanning electron microscope and transmission electron microscope was extensively used to explore the morphological and structural properties. Electrical properties of MWCNT suggest semiconducting behavior. Infrared (IR) radiation detection is demonstrated using MWCNT and prototypes of room temperature and low temperature. IR radiation detectors have been made using different morphologies of MWCNT as the active sensor material.

1. Introduction

Carbon nanotubes are the graphene sheets rolled into empty cylindrical shapes. Each nanotube is made up of a sp^2 covalently bonded carbon atoms. These carbon nanotubes (CNT) are 1D nanostructures which have significant advantages over many existing nanostructured materials due to their unique mechanical, electronic, optical and chemical properties [1–3]. The electronic properties of CNT are very sensitive to the geometric structure. Coaxial multiwall nanotubes can be metallic or semiconducting depending upon the diameter which, in turn, is inversely proportional to bandgap energies. In semiconducting CNT, the energy band gap ranges between 0.4 and 6 eV [4]. The diameter of multiwalled carbon nanotubes (MWCNT) is typically in the range of few tens of nanometers with maximum length of hundreds of microns and can be calculated using the equation,

$$d_t = \left[\frac{a(m^2 + mn + n^2)^{1/2}}{\pi}\right] = \frac{C_h}{\pi}$$

where C_h is the length of chiral vector, and a is the lattice constant of graphite [5]. The bandgap 'E_g' of a semiconducting nanotubes is given by $2d_{C-C}\gamma/D$ where $d_{C-C} = 0.142$ nm is C—C bond length, γ is the nearest-neighbor hopping parameter and is equal to 2.5–3.2 eV and D is the nanotube diameter [6,7]. Various synthetic methods have been developed for the production of CNTs, including arc discharge [8], laser ablation [9], plasma enhanced [10] and thermal chemical vapor deposition (CVD) [11]. CVD has been the preferred method among different methods because of its potential advantage to produce a large amount of CNTs growing directly on a desired substrate with high purity, controlled growth, morphology and large yield [12]. Simple and complex morphologies, i.e. carbon nanocoils [5] can be synthesized either by applying a magnetic field in the reaction zone or by using sputtered thin films of Au and Au/Ni as catalysts. Controlled and aligned growth of CNTs has many applications in electronic devices and composite materials. Carbon nanotubes production using CVD method requires the catalyst nanoparticles on the substrate during or before the synthesis of nanotubes [11].

The photoconductivity of single walled carbon nanotubes has absorption peaks in infrared region that show electronic interband transitions [13]. This indicates that CNT due to photoconductivity and wide range of bandgaps are potential candidates for fabrication of radiation detectors [14–17]. Later on multiwalled carbon nanotubes were used for IR sensing due to fabrication issues associated with the use of single-walled CNT. Single-walled CNT have low quantum efficiency due to their extremely small diameter (0.4–2.5 nm) and short absorption depth. On the other hand MWCNT based infrared sensors have been reported to show higher quantum efficiency [18]. Many researchers have already worked

* Corresponding author at: Alamoudi Water Chair, King Saud University, P.O. Box 2460, Riyadh, Saudi Arabia. Tel.: +966 1 4673739; fax: +966 1 4673739.
E-mail addresses: umanzoor@ksu.edu.sa, umanzoor@comsats.edu.pk (U. Manzoor).

0924-4247/$ – see front matter © 2012 Elsevier B.V. All rights reserved.
http://dx.doi.org/10.1016/j.sna.2012.08.028

on the bolometric effects [19] of CNTs making extensive efforts towards utilisation of either single-walled carbon nanotubes [20] or multiwalled carbon nanotubes in the form of randomly, aligned or suspended films for the detection of infrared radiation. To our knowledge, no infrared sensor has been made so far using coiled or twisted MWCNT.

In this research, growth of MWCNT using catalytic CVD technique is reported. A parametric study of various factors influencing growth of carbon nanotubes is performed. Specifically, the effect of composition mixture of hydrocarbon and inert gases as feed source to reactor is studied. Analysis of the prepared CNTs was done using SEM and TEM [21,22]. Electrical parameters of the grown CNTs are also studied. IR detectors were fabricated and tested for exploration of MWCNT as active IR detector material.

2. Experimental procedure

MWCNT were grown using chemical vapor deposition technique. This technique involves dissociation of hydrocarbon molecules catalyzed by transition metal and dissolution and saturation of carbon atoms on the metal nanoparticle. The precipitation of carbon from the saturated metal particle leads to the formation of nanotubes. Catalyst nanoparticles (mixed ferrite of the composition, $Co_{0.5}Zn_{0.5}Fe_2O_4$) were synthesized by chemical route [23] due to the ability of iron based nanoparticles towards growth of carbonaceous tubes with high efficiency.

For CNT growth, a quartz tube (Ø 30) was placed inside a tube furnace. The substrates were etched for 60 min in 5.0 M NaOH solution. Catalyst-supported substrates were prepared by dipping substrates in 2.7 mM colloidal suspensions of nanoparticles in ethanol. Prior to that, each suspension was subjected to ultrasonic vibration for 10 min to ensure deflocculation of soft agglomerates. These substrates were placed inside an alumina boat and loaded into the quartz tube. The heating to the synthesis conditions (10 sccm Ar flow, 680 °C, 15 min) and post-synthesis cooling were carried out under constant argon flow which served as a carrier gas and provided inert atmosphere as well. Acetylene (C_2H_2) was used as the precursor gas for CNT synthesis through thermal cracking. Different ratios of C_2H_2 and Ar gas were carefully

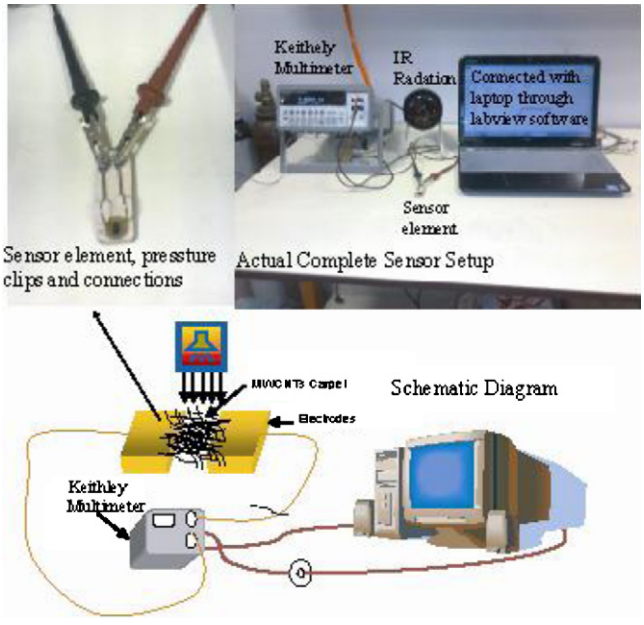

Fig. S1. (a) Actual sensor element with pressure clips and connections. (b) Actual complete sensor setup with IR lamp. (c) Schematics of complete setup for infrared sensor and its testing.

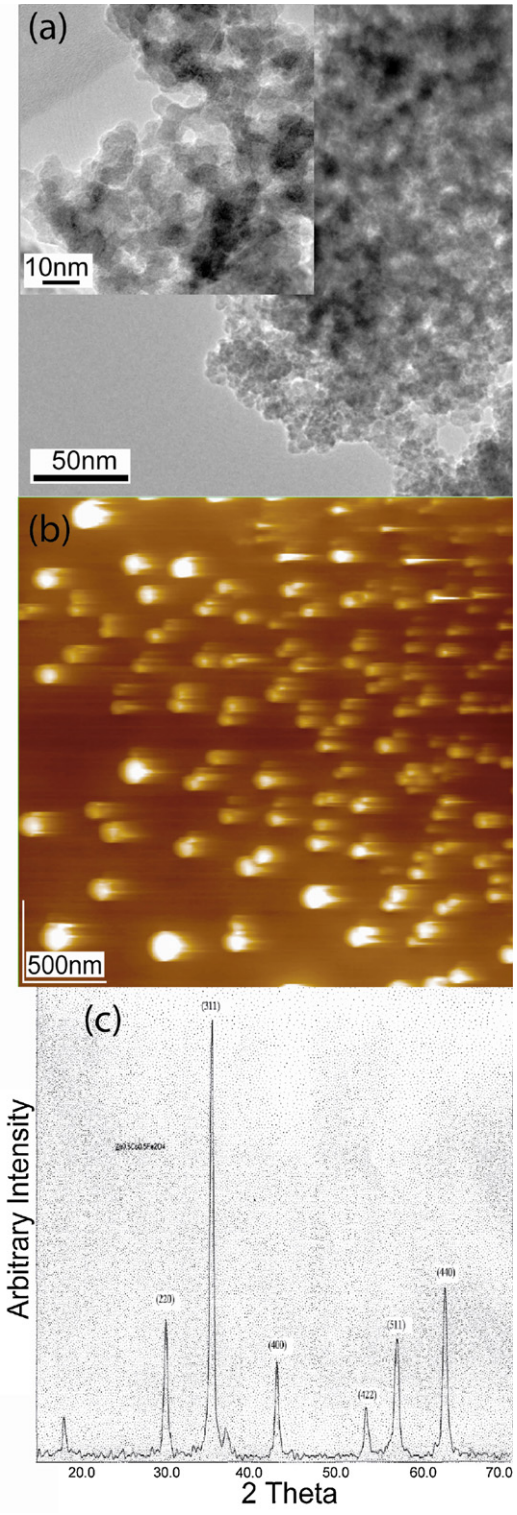

Fig. 1. (a) Low and high (inset) magnification TEM images of catalyst nanoparticles. (b) AFM image of catalyst suggesting discrete and agglomerated nanoparticles. (c) X-ray diffraction spectrum with indexed peaks for mixed ferrite nanoparticles.

controlled to get different morphologies. The flow rate of acetylene was maintained by using a digital mass flow controller (Make and Model, e.g. MKS 247C). The morphological and structural characterization of nanoparticles and nanotubes was performed using atomic force microscope (JEOL, Model SPM5200), x-ray diffractometer (STOE, Stadi MP), scanning electron microscope (JEOL,

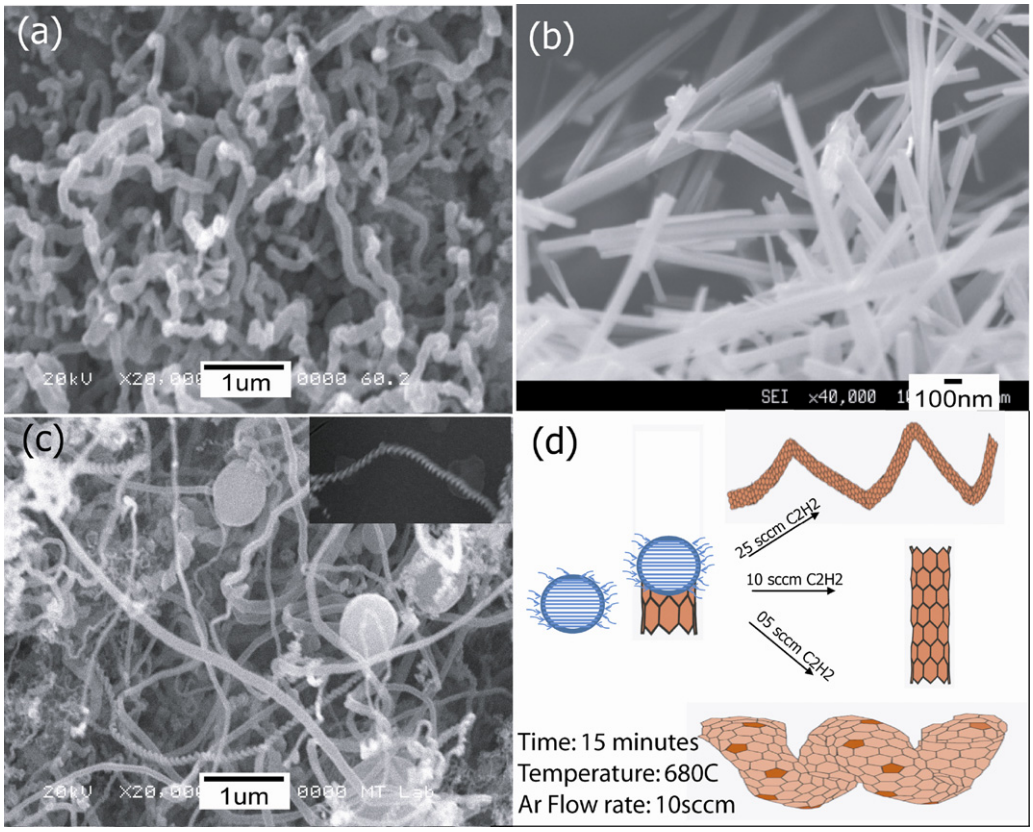

Fig. 2. SEM images of MWCNT. (a) Randomly oriented CNT of average diameter 145 ± 44 nm with 25 sccm of C_2H_2. (b) Rigid and highly crystalline CNT of average diameter 67 ± 27 nm with 10 sccm of C_2H_2. (c) Twisted CNT of average diameter 75 ± 30 nm with 5 sccm of C_2H_2 diluted with 10 sccm of inert gas with the inset showing an individual twisted MWCNT, and (d) Schematic illustration of different growth morphologies obtained from different C_2H_2 flow conditions.

Model JSM6460), and high-resolution transmission electron microscope (Hitachi HNAR9000 microscope).

The infrared radiation detectors were fabricated by depositing 50-nm thick gold electrodes onto glass substrates through sputter deposition technique and MWCNT were placed between electrodes (through doctor blading). The sensitivity of the device was measured by observing the resistance behavior on illumination of infrared radiation on the device. The resistance was measured using a source meter (Keithley, model 2000). Fig. S1 is the schematic presentation of the sensor setup for testing and data recording.

The detector was fabricated by depositing 50-nm thick gold electrodes onto quartz substrates through sputter deposition technique. The linear dimensions of this prototype with electrodes are L = 8 mm; W = 6 mm and the separation between the electrodes (along the length) was 1 mm. MWCNT were scratched from the substrate and placed between electrodes through doctor blading. The connections from electrodes to the Keithley multimeter (model 2000) were made by conducting metallic pressure contacts. A 100 W infrared lamp was used for irradiation of infrared light on the detector.

3. Results and discussion

Fig. 1(a) shows the high magnification transmission electron microscope (TEM) image while the inset represents low magnification view of the catalyst nanoparticles (NP). From HRTEM studies, the average nanoparticle size was estimated to be 9.7 ± 2.0 nm. Atomic force microscope (AFM) studies of the powder revealed information regarding particle size and agglomeration. Uniform dispersion of nanoparticles over atomically smooth surface of highly oriented pyrolytic graphite was noticed as shown in 2 μm scan of the surface (Fig. 1b). It is anticipated that few relatively more bright particles in the AFM image are the agglomerated particles. Examination of catalyst nanoparticles under TEM also revealed formation of nanoparticles clusters. Fig. 1(c) is the X-ray diffraction spectrum of the catalyst nanoparticles. The formation of face-centered cubic structure with peaks characteristic of mixed ferrite powder of the composition $Co_{0.5}Zn_{0.5}Fe_2O_4$ was confirmed. Using Scherrer equation [24], the average NP size was computed to be 19.1 nm. The phenomenon of peak broadening also indicated crystallite size to be in the nanoscale regime. The results clearly suggest that the catalyst particles are highly crystalline with size of the order of few nanometers, as confirmed by XRD, AFM, and TEM studies.

Among a wide range of growth conditions explored for nanotube synthesis, the C_2H_2:Ar gas flow ratio was found to strongly influence characteristics of carbonaceous deposit obtained. Scanning electron microscope (SEM) images of the samples after synthesis at 680 °C for 15 min under different flow conditions are presented in Fig. 2. All the SEM microstructures clearly suggest formation of different morphologies of MWCNT with very small amount of soot formation. A relatively high flow rate of 25 sccm for pure C_2H_2 gas resulted in growth of randomly oriented MWCNT with a large diameter of 145 ± 44 nm. Although the nanotube diameter was uniform for most of the MWCNT, a small fraction of nanotubes were found to have sub-100 nm diameter as well. Also, precise measurement of nanotube length was not possible due to spaghetti-like appearance of nanotubes. As C_2H_2 flow rate was reduced to 10 sccm, rigid and straight nanotubes with much less diameter, albeit with much diversity in characteristics, were produced. From Fig. 2(b), the average value of nanotube diameter was estimated to be 67 ± 27 nm.

The CNTs are stiff (rod-like) and any curvature along their length or entanglement between them is missing. This rigidity of CNT [25] clearly suggests high crystallinity because defect free/low defect structures are often seen as straight or elastic bending structures [26]. Another prominent growth feature was the presence of twisted/coiled MWCNT when the hydrocarbon flux rate was further reduced to 5 sccm. Fig. 1(c), shows SEM microstructures of twisted CNTs with an average value of the outer diameter to be 75 ± 30 nm. The enlarge SEM image of an individual, isolated twisted/coiled MWCNT is shown in inset of Fig. 2(c). The coiled MWCNT produced consist of pentagons and heptagons with formation of hexagonal network in the growing structures at initial stages [11]. The transition in MWCNT morphology, from initially curved, randomly-oriented to straight, rigid to eventually twisted/coiled structures, upon gradual decrease and subsequent dilution of precursor C_2H_2 gas flow maybe attributed to the change in the incident carbon flux over the catalyst surface.

These twisted CNT are unique and the growth mechanism can be attributed to (i) impurities in gas composition [11,27] and/or (ii) different catalyst crystal planes that lead to anisotropy in carbon deposition onto the growing nanotube end [28]. It is accepted that the concentration or the flow rate of reactive gas plays an important role in the morphology of coiled structures but in this report the morphology is completely changed from random CNTs to rigid structures and further change in gas flow produces coiled shape morphology [27]. If the impurities are responsible then with the increase in C_2H_2 flow rate, there will be an increase in the impurities, resulting in better quality of coiled CNT. However, the morphology completely changes by varying the flow rate. It is believed that the formation of coiled nanotubes depends critically on catalyst clusters modified by surface effects and the nonsymmetrical fashion of diffusion path lengths in the catalyst nanoparticles. It is therefore proposed that, in our case, growth of carbon nanocoils is dependent on different crystal/cluster surfaces of the catalyst (anisotropic characteristics of the crystal faces due to different surface energies) [28]. This argument is further strengthened by the high crystallinity of the catalyst particles as shown in X-ray diffraction (XRD) results, and the presence of small clusters suggested by the AFM image (Fig. 1). Also, no coiled structures were seen when the catalyst was changed to Fe, Fe_2O_3 and Fe doped ZnO with flow rates of 5, 10 and 25 sccm (results not shown). At the same time, variation in the incident carbon flux at the catalyst NP surfaces (due to the above-mentioned reason) or at the tip of growing CNT results in variation in the MWCNT outer diameter along its length or growth of helical nanotubes or both.

TEM investigation of the nanotubes produced under diluted C_2H_2 precursor flow conditions confirmed synthesis of MWCNT with diameters, typically in the range of 30 to 50 nm (Fig. 3b). The rigid nanotubes were highly crystalline with clear indication of fringes representative of multiple coaxial graphene shells. From section of the randomly grown MWCNT shown in Fig. 3a, the nanotube was determined to have been made up of ~20 walls with inter-shell spacing of 0.34 nm. As stated earlier and also noticed during TEM examination, changes in localized incident carbon flux induces a change in the nanotube diameter. The inside diameter of the nanotube was estimated to be ~12 nm which is in the same range as those of catalyst nanoparticles used. It is anticipated that, prior to CNT growth, the size of the catalyst nanoparticles decreases slightly due to reduction from oxide state to metallic form caused by the presence of hydrogen from thermal decomposition of C_2H_2 molecules.

Electrical characterization of rigid CNT are shown in Fig. 4. There is a linear low field region from 0 to 0.3 V after which the *I–V* behavior is non-linear. This may be due to factors such as conduction through more sub-bands, tunneling to inner tube shells and hopping between localized states. This semi-metallic behavior suggests presence of both semiconducting and metallic nanotubes.

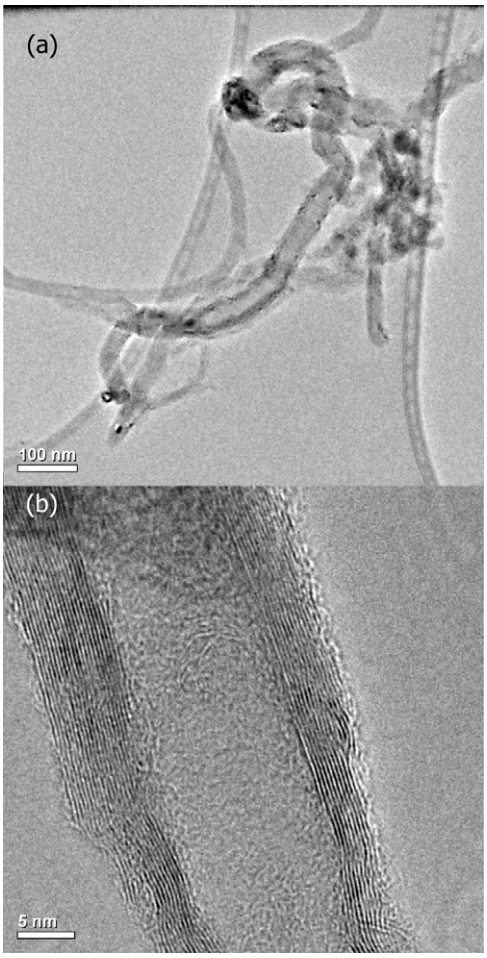

Fig. 3. High resolution TEM microstructures of (a) randomly-oriented nanotube and (b) a highly crystalline, rigid MWCNT.

Fig. 5 results from testing of home-made sensors produced using doctor-blading process. IR radiation sensors were developed by

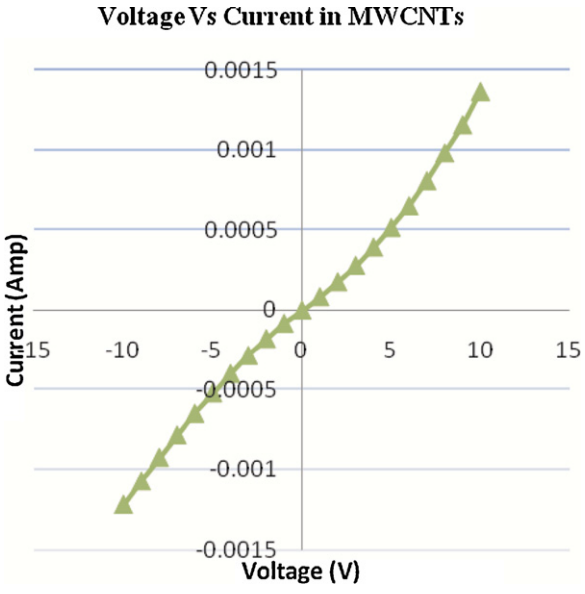

Fig. 4. *I–V* characteristic curve of randomly grown MWCNT.

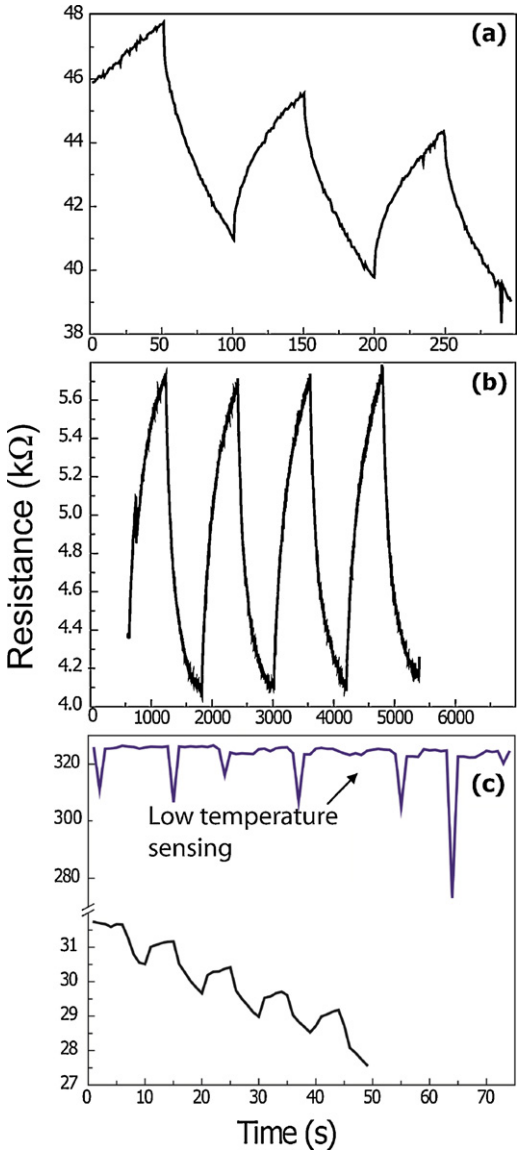

Fig. 5. Time-dependent changes in electrical resistance upon exposure to IR radiation for MWCNT based detectors made from (a) randomly-oriented nanotubes. (b) highly crystalline, rigid CNTs, and (c) coiled/helical nanotubes.

using thick layer of CNT as active layer between two electrodes. The response was observed by making individual sensors for different morphologies. With MWCNT deposition over glass slides in the area between two gold electrodes and illumination with IR lamp, a fast decrease in resistance was observed whereas an increase in electrical resistance was noticed when the infrared radiation was turned off. This behavior suggests fast device response in the IR regime.

The MWCNTs dispersion between electrodes that also function as electrical contacts is illuminated by 100 W infrared lamp. The overall decrease in resistance was observed at room temperature. This is a clear indication that directs photoconductivity can contribute photoexcited carriers to the electric field and response can be bolometric in nature in which the absorbed radiation heats the sample. The photoresponse is increased when this effect is minimized by operating the device in vacuum and low temperature conditions (Fig. 5c). In a recent study Mikhail et al. showed photoresponse of single-walled carbon nanotube films in but the overall sensitivity was very low [19]. Recently Gohier et al. [29] fabricated MWCNT Based IR sensors but again the sensitivity was very low and the sensitivity reported in this paper is much better than the above-mentioned paper.

Fig. 5 clearly suggests that all the 3 morphologies (randomly oriented, rigid and coiled MWCNT) show response to the IR radiations. Sensitivity ($R = R_{black}/R_{IR}$) of randomly oriented and coiled MWCNT is 1.1 and rigid CNTs show response of 1.4. Highest change in resistance response (sensitivity) was observed for the rigid CNT. The response is largely restricted by internal defects and different optical scattering mechanisms of the MWCNT samples, including surface scattering (both specular and diffuse), small particle scattering, and volume scattering [30]. It is expected that all the above-mentioned phenomena are responsible for decreasing the quantum efficiency of the IR sensor. However, the possible reason for this higher response can be attributed to the better crystallinity of these structures. It was also suggested that the coiled CNT formation mechanism is because of the defects and therefore it shows lowest response to IR radiations. Room temperature sensing results show that with the series of on-off illumination, the rise and decay for equal interval of time was observed. This overall decrease in resistance with passage of time was may be due to atmospheric and thermal effect (Fig. 5). The overall thermal effect was reduced when device with coiled MWCNT film was tested in a vacuum chamber at temperature 40 K. The several off-on stable states are observed and the coiled MWCNT showed steady response to IR in vacuum as shown in Fig. 5c. However, according to our understanding, MWCNT for IR detection are still at the developmental stage [31]. More in-depth research work is needed to answer questions i.e. (i) how to fine tune the CNT for minimizing the dark current and maximizing the absorption, and (ii) how to get peak quantum efficiency, which is directly related to absorption and surface reflections.

4. Summary

Morphology can be controlled by carefully controlling flow rates of hydrocarbon. Randomly oriented, rigid and coiled MWCNT were successfully synthesized. The effect of catalyst on formation mechanism of coiled CNT is important. The developed prototype sensors have good response towards IR radiations. The overall decrease in resistance, during the on-off cycles can be controlled by conducting experiments at low temperature.

Acknowledgements

The authors are grateful to Mr. Nicolas Gautier at Institut des Materiaux (IMN), Universite de Nantes, France, for assistance with HRTEM studies. The research grant from Higher Education Commission, Pakistan through its National Research Program for Universities is gratefully acknowledged. This work was also financially supported through the “Projects & Research” axis of the Alamoudi Water Chair (AWC) at King Saud University, Riyadh, Saudi Arabia.

References

[1] J. Han, Structures and Properties of Carbon Nanotubes, CRC Press, New York, 2004.
[2] Q. Zhang, M.Q. Zhao, D.M. Tang, F. Li, J.Q. Huang, B. Liu, W.C. Zhu, Y.H. Zhang, F. Wei, Carbon-nanotube-array double helices, Angewandte Chemie International Edition 49 (2010) 3642–3645.
[3] M.D. Volder, S.H. Tawfick, S.J. Park, D. Copic, Z. Zhao, W. Lu, A.J. Hart., Diverse 3D microarchitectures made by capillary forming of carbon nanotubes, Advanced Materials 22 (2010) 4384–4389.
[4] M.S. Dresselhaus, G. Dresselhaus, P. Avouris, Carbon Nanotubes: Synthesis, Structure, Properties and Applications, Springer, Heidelberg, 2001.
[5] W.H. Chiang, D.N. Futaba, Growth control of single-walled double-walled, and triple-walled carbon nanotube forests by a priori electrical resistance measurement of catalyst films, Carbon 49 (2011) 4368–4375.
[6] C. Seah, S.P. Chai, A.R. Mohamed, et al., Synthesis of aligned carbon nanotubes, Carbon 49 (2011) 4613–4635.

[7] X. Devaux, S.Yu Tsareva, A.N. Kovalenko, Formation mechanism and morphology of large branched carbon nano-structures, Carbon 47 (2009) 1244–1250.
[8] C. Kuzuya, W. In-Hwang, S. Hirako, Preparation, morphology and growth mechanism of carbon nanocoils, Chem. Vap. Dep. 8 (2002) 57–62.
[9] A. Volodin, M. Ahlskog, E. Seynaeve, Imaging the elastic properties of coiled carbon nanotubes with atomic force microscopy, Physical Review Letters 84 (15) (2000) 3342–3345.
[10] Z.P. Huang, J.W. Xu, Z.F. Ren, J.H. Wang, M.P. Siegal, P.N. Provencio, Growth of highly oriented carbon nanotubes by plasma-enhanced hot filament chemical vapor deposition, Applied Physics Letters 73 (1998) 3845–3847.
[11] D. Fejes, K. Hernádi, A review of the properties and CVD synthesis of coiled carbon nanotubes, Materials 3 (2010) 2618–2642.
[12] K.T. Lau, M.L. Hui, Coiled carbon nanotubes: synthesis and their potential applications in advanced composite structures, Composites: Part B 37 (2006) 437.
[13] M.A. El Khakani, V.L. Borgne, B. Aïssa, F. Rosei, C. Scilletta, E. Speiser, et al., Photocurrent generation in random networks of multiwall-carbon-nanotubes grown by an all-laser process, Applied Physics Letters 95 (2009) 083114–83116.
[14] U. Coscia, G. Ambrosone, A. Ambrosio, M. Ambrosio, F. Bussolotti, V. Carillo, et al., Photoconductivity of multiwalled CNT deposited by CVD, Solid State Sciences 11 (2009) 1806–1809.
[15] B. Pradhan, K. Setyowati, H. Liu, D.H. Waldeck, J. Chen, Carbon nanotube–polymer nanocomposite infrared sensor, Nano Letters 8 (2008) 1142–1146.
[16] F. Akihiko, M. Yasuyuki, H. Suematsu, N. Ogawa, K. Miyano, H. Kataura, et al., Photoconductivity in semiconducting single-walled carbon nanotubes, Japanese Journal of Applied Physics 40 (2001) L1229–L1231.
[17] A. Ugawa, J. Hwang, H.H. Gommans, H. Tashiro, A.G. Rinzler, D.B. Tanner, Far-infrared to visible optical conductivity of single-wall carbon nanotubes, Current Applied Physics 01 (2001) 45–49.
[18] L. Liu, Y. Zhang, Multiwalled carbon nanotube as a new infrared detected material, Sensors and Actuators A 116 (2004) 394–397.
[19] M.E. Itkis, F. Borondics, A. Yu, R.C. Haddon, Bolometric infrared photoresponse of suspended single-walled carbon nanotube films, Science 312 (2006) 413–416.
[20] P.W. Barone, S. Baik, D.A. Heller, M.S. Strano, Near-infrared optical sensors based on single-walled carbon nanotubes, Nature Materials 4 (2005) 86–92.
[21] S.P. Chai, A.R. Mohamed, C. Ming, Synthesis of aligned carbon nanotubes, Carbon 49 (2011) 4613–4635.
[22] X. Devaux, S.Y. Tsareva, A.N. Kovalenko, E.V. Zharikov, E. McRae, Formation mechanism and morphology of large branched carbon nano-structures, Carbon 47 (2009) 1244–1250.
[23] R.A. Urugana, G. Vaidyanathan, S. Sendhilnathan, Preparation and properties of temperature-sensitive magnetic fluid having $Co_{0.5}Zn_{0.5}Fe_2O_4$ and $Mn_{0.5}Zn_{0.5}Fe_2O_4$ nanoparticles, Physica B 368 (2005) 223.
[24] P. Scherrer, Bestimmung der Größe und der inneren Struktur von Kolloidteilchen mittels Röntgenstrahlen, Nachr d Ges d Wiss zu Göttingen Math-Phys Kl (1918) 98–100.
[25] C. Ni, C. Deck, K.S. Vecchio, P.R. Bandaru, Optical determination of the flexural rigidity of carbon nanotube ensembles, Applied Physics Letters 92 (2008) 173106.
[26] A. Volodin, M. Ahlskog, E. Seynaeve, C.V. Haesendonck, Imaging the elastic properties of coiled carbon nanotubes with atomic force microscopy, Physical Review Letters 84 (2000) 3342–3345.
[27] D. Li, L. Pan, Y. Wu, W. Peng, The effect of changes in synthesis temperature and acetylene supply on the morphology of carbon nanocoils, Carbon 50 (2012) 2571–2580.
[28] L. Pan, M. Zhang, Y. Nakayama, Growth mechanism of carbon nanocoils, Journal of Applied Physics 91 (2002) 10058.
[29] A. Gohier, A. Dhar, L. Gorintin, P. Bondavalli, Y. Bonnassieux, C.S. Cojocaru, All-printed infrared sensor based on multiwalled carbon nanotubes, Applied Physics Letters 98 (2011) 063103.
[30] K.T. Lau, L. Mei, D. Hui, Coiled carbon nanotubes: synthesis and their potential applications in advanced composite structures, Composites: Part B 37 (2006) 437–448.
[31] X.J. Wang, J.D. Flicker, B.J. Lee, W.J. Ready, Z.M. Zhang, Visible and near-infrared radiative properties of vertically aligned multi-walled carbon nanotubes, Nanotechnology 20 (2009) 215704.